Analysis of Fuel Burn-up Calculations of 3600 MWth Sodium-cooled Fast Reactor Core

Amr Ibrahim

High Institute for Engineering and Technology at Obour, Cairo, Egypt.

A R T I C L E   I N F O

A B S T R A C T

Fast spectrum reactors are essential for the future of nuclear energy. Therefore, there is a need for continuous research and development of the design and safety of current and future nuclear fast reactors. The aim of this work is to analyze the process of fuel burnup in a large scale (3600 MWth) Sodium cooled Fast Reactor (SFR) core. This design is called European Sodium Fast Reactor (ESFR). It is proposed in the 7th Framework Programme within the Euratom Framework. A new version (version 2.7) of Monte Carlo neutron transport code (MCNPX) was used to design a 3D model of the ESFR core to evaluate and analyze a number of burnup-relevant characteristics. These include the flux and power distributions across the ESFR core as well as the reactivity changes and fuel transmutation during burnup to take into account the changes in fuel composition during burnup. Obtained results can serve as up to date evaluation for the design and well allow for a detailed assessments of the fuel performance inside the ESFR core.

1.   INTRODUCTION

The Sodium-cooled Fast Reactor (SFR) is one of the most promising advanced systems that are expected to fulfill the declared goals of the Generation-IV International Forum (GIF), in particular those related to sustainability and safety **[1]**. Nearly 60 years of technological and scientific experience gained from related projects in many countries have gained SFR a unique position between the different systems considered in the GIF. Many countries achieved significant technological advancements of sodium-cooled fast reactors not only in terms of operation but also in terms of design. The EBR (Experimental Breeder Reactor) and the FFTF (Fast Flux Test Facility) in USA, the series of BN systems in Russia, the Monju reactor in Japan and the commercial Super Phénix in France have added over 400 years of operational experience in the technology of SFR **[2]**. Latest members of sodium-cooled reactors are the China Experimental Fast Reactor (CEFR) recently connected to the grid **[3]**, in Russia the BN-800 reactor **[4]** and in India the PFBR (Prototype Fast Breeder Reactor) **[5]**. In Europe, the ESNII "European Sustainable Nuclear Industrial Imitative" has carried out an industrial project for demonstration purposes called "Advanced Sodium Technological Reactor" (ASTRID).

Along with the current under construction fast reactor projects, many countries in Europe are conducting research programs for the improvement of fast reactors and generation IV concepts.

The SFR design considered in this work is called European Sodium Fast Reactor (ESFR). It is based on the European Project CP-ESFR (Collaborative Project on the European Sodium Fast Reactor). CP-ESFR started as part of the EURATOM contribution to the GIF and as a first step to create a common European framework for supporting the sodium fast reactor technology. It was launched within the 7th EURATOM Framework programme. This programme groups 24 European partners with the objective to establish the technical basis of European sodium cooled fast reactor (ESFR) plant with improved performance, safety, resource efficiency and cost reduction **[6]**.

The design and safety analysis of current and future nuclear reactors, during normal operation and under accidental situations, requires continuous research and also improvement of computational accuracies. In this work, a new version (version 2.7) of Monte Carlo neutron transport code MCNPX **[7]** was used to design a 3D model of the ESFR core to evaluate and analyze a number of burnup-relevant characteristics. These

included flux and power distributions in the ESFR core as well as the changes in core reactivity and fuel isotopic composition during fuel cycle (2050 effective full power day). Furthermore, the characteristics of both flux and power were investigated both for the beginning of life (BOL) as well as the end of cycle (EOC) conditions to take into consideration the changes in fuel isotopic composition during burnup. Obtained results will serve as an up to date analysis for further assessments of fuel behavior and performance in the ESFR core.

1.2. Model Description

The design used for the calculations of this study is a detailed 3D European Sodium Fast Reactor oxide core model. The geometry details of this core were reproduced, using MCNPX, fully resolved in three dimensions (axially and radially) as set in the design specification **[8]**. The ESFR core parameters are presented in Table 1.

Table (1): The ESFR oxide core parameters

Parameter	Value
Thermal power	3600 MWth
Lattice pitch	20.08 cm
Fuel type	MOX
No. of fuel assemblies	453
Volume	17.5 m^3
Diameter	4.72 m
Height	1.00 m
Height/Diameter Ratio	0.21
Average burn up	~100 GWd/tHM
Inlet coolant temperature	395 ºC
Outlet coolant temperature	545 ºC
Pressure drop	0.1 MPa

The ESFR core layout is composed of an inner and outer fuel zone. Each zone has different Plutonium (Pu) content. There are 228 outer fuel assemblies and 225 inner fuel assemblies. The control rod system of the reactor is composed of two main devices: the Control and Shutdown Device (CSD) which is formed of 24 CSD assemblies and the Diverse Shutdown Device (DSD) which is formed of 9 DSD assemblies. In the designed model, both the CSD and DSD are withdrawn from the active core. Radial Reflector around active core is formed of 331 assemblies representing three rings around the core plus to one reflector assembly located in

the middle of the core. The reflectors are made of structured material (steel) **[9]**. Fig. 1 shows horizontal layout of the MCNP model at fuel level. Three radial zones are noticeable in the horizontal layout of the ESFR core. The first zone (in blue) is the inner core (IC) fuel zone while the second radial zone (in cyne) is the outer core (OC) fuel zone. The third zone (in red) depicts the radial reflector. A single sub-assembly of the reflector is also present in the very center of the core. The CSD and DSD rods are situated scattered in the two fuel zones as shown.
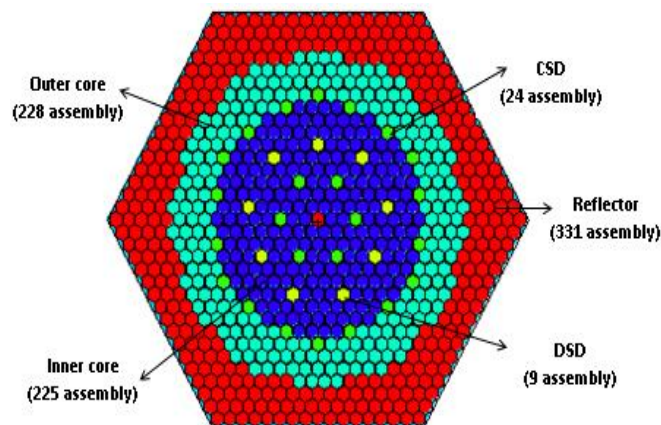

Fig. (1): Horizontal layout of the MCNP ESFR core model.

1.2.1 ESFR Fuel Assembly

Each fuel assembly contains 271 fuel pins. The pins are fixed by helical wire wrap spacers and made of mixed oxide fuel (MOX) pellets while cladding is formed of Oxide Dispersion Strengthened (ODS) steel. To flatten the core radial power profile, the outer fuel assemblies have an increased fraction of Pu (~17 wt.%) compared to the inners (14.05 wt.%). The uranium vector in the $(U,Pu)O_2$ fuel is depleted uranium while the plutonium vector is estimated as one coming from ~4500 MWd/tHM burnup, after 20 years cool down. As a consequence, a small fraction of Am-241 coming from Pu-241 decay is considered. The fuel average density of the mixed oxide fuel (MOX) is 9.95 g cm^{-3}. This is 90% of the TD (Theoretical Density) accounting for the porosity of the fuel pellet. The isotopic mass fractions of the fuel in the two core zones (at BOL) are depicted in Table 2. The vertical and horizontal layouts of the fuel assembly and fuel pin are shown in Fig. 2 while Table 3 presents the fuel assembly dimensions (at room temperature). In the horizontal layout of the fuel assembly, the fuel pins are illustrated in blue while the green color corresponds to the sodium coolant. The orange color refers to structural material. The initial temperatures and densities of the MCNP model are given in Table 4.

Table (2): Isotopic mass fractions of the fuel in the two core zones at BOL [10].

Isotopes	Inner fuel zone (w%)	Outer fuel zone (w%)
U-235	0.19	0.18
U-238	75.09	73
Pu-238	0.46	0.54
Pu-239	6.12	7.11
Pu-240	3.83	4.45
Pu-241	1.06	1.24
Pu-242	1.34	1.56
Am-241	0.1	0.17
O-16	11.81	11.75

Fig. (2): Horizontal and vertical layout of the ESFR fuel assembly and fuel pin.

Table (3): ESFR fuel assembly dimensions [10]

ESFR fuel assembly parameter	value
Assembly pitch	21.08 cm
Sodium gap between assemblies	0.45 cm
Thickness of Assemblies wrapper tube	0.45 cm
Wire wrap spacer radius	0.1 cm
Number of fuel pins in fuel assembly	271
Fuel pin pitch	1.173 cm
Outer clad diameter	1.73 cm
Inner clad diameter	0.973 cm
Fuel pellet diameter	0.943 cm

Table (4): Temperatures and densities of the ESFR core materials [10].

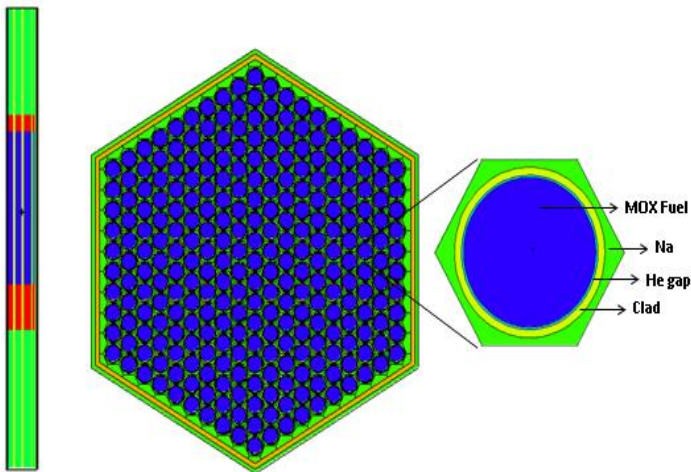| parameter	value
MOX Fuel Temperature	1500 K
Coolant and structural materials temperature	743 K
BC_4 Absorber temperature	900 K
MOX Fuel density	9.95 g cm^{-3}
Sodium Coolant density	0.84 g cm^{-3}
ODS steel density	7.25 g cm^{-3}

2. MODELING CODE AND METHODOLOGY

MCNP (Monte Carlo N-Particle code) is a multipurpose and a powerful computational tool for particle transport calculations. It can be used for neutron transport, criticality and burnup calculations. MCNP is able to calculate the effective multiplication factor (keff), reaction rates, neutron fluxes, power peaking factors, and reaction rate distributions, etc. [7]. The stochastic neutron transport and criticality in this work is performed using continuous energy cross-sections corresponding to data from the default MCNPX ENDF/B-VII cross-sections library [11]. This library include data for all core relevant isotopes at several temperatures in the range of 300 to 1800 K. MCNPX version 2.7 was used to simulate the transport of neutron inside the ESFR core. The accuracy of the obtained results using MCNP simulation mainly depend on the number of neutrons histories. To have results with a reasonable statistical error using MCNPX, one must have a good estimation of the required number of neutrons per cycle and the total number of cycles in the burnup calculations. The calculations in this work were performed using a 20000 source histories per cycle, with a total number of 150 cycles (125 active cycles and 25 to be skipped). A burnup card is used to burn the fuel in one irradiation batch up to 2050 days which corresponds to 99 GWd/T. The cycle time was divided into 16 time steps. It should be noted that, in all the presented simulations, the control rods are located in their upper parking positions

3. RESULTS AND DISCUSSION

3.1 Neutron Flux and Power Distribution

The F4 combined with FM tallies in MCNP5 [12] have been employed to determine the radial distribution of both the neutron flux and power at the beginning of core life as well as at EOC. Both distributions have been

measured at the midway point between the bottom and the top of the active fuel region. Scaling factors were applied in order to normalize the results of both the flux and power by the thermal power of the ESFR core [13]. Furthermore, the flux results have been partitioned into three energy groups, with boundaries 0.625 eV (thermal flux), 0.625 eV - 0.1 MeV (intermediate flux) and > 0.1 MeV (fast flux) in order to evaluate the contribution of neutrons belonging to each energy group to the ESFR total neutron flux.

Fig. 3 shows the radial distribution of neutron flux (thermal, intermediate, fast and total flux) at BOL as well as the total radial flux distribution at EOC. As shown the total flux at BOL is not very flat across the core. It is clear that the flux profile demonstrates the highest values in the outer core where the fuel enrichment is high. However, the total power profile is much more flattened at the EOC as during burnup the initial enrichment of the outer core decreases. As shown at BOL the thermal neutron flux within the core is negligible and the total flux is mainly formed of neutrons at intermediate and fast energy ranges with the fast flux being higher which is favorable for a fast spectrum concept. However, the intermediate flux becomes higher at the periphery of the active core due to the moderation effect of the radial reflector region.
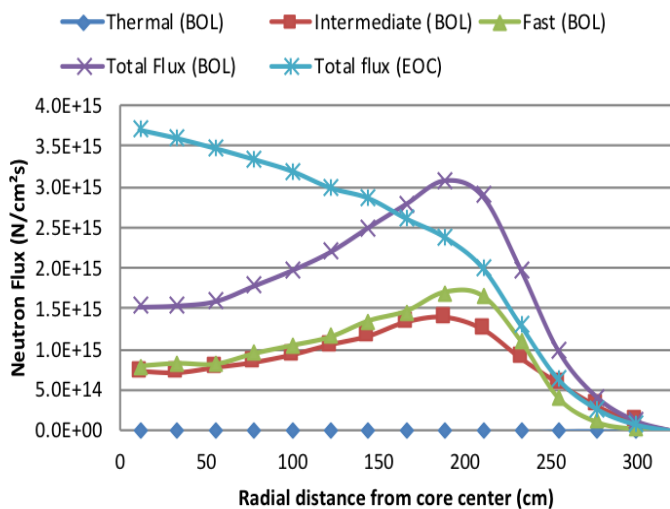

Fig. (3): Radial neutron flux distribution of the ESFR at BOL and EOC conditions.

MCNP5 neutronic calculations showed that the percentage contribution of neutrons in the fast, intermediate, and thermal neutron ranges to the fission reaction at BOL is equal to 58.18%, 42.81% and 0.01%, respectively. These percentages are consistent with the obtained radial flux spectrum. Fig. 4 compares the power peaking factor of the ESFR core at BOL and at EOC. It is clear from Fig. 4 that the total power profile follows the profile of the total radial flux as expected. Also, the

core total power is much more flattened at the EOC. The power peaking factor decrease from 1.6 at BOL to 1.25 at the EOC and it tend to be more flat which is desirable.
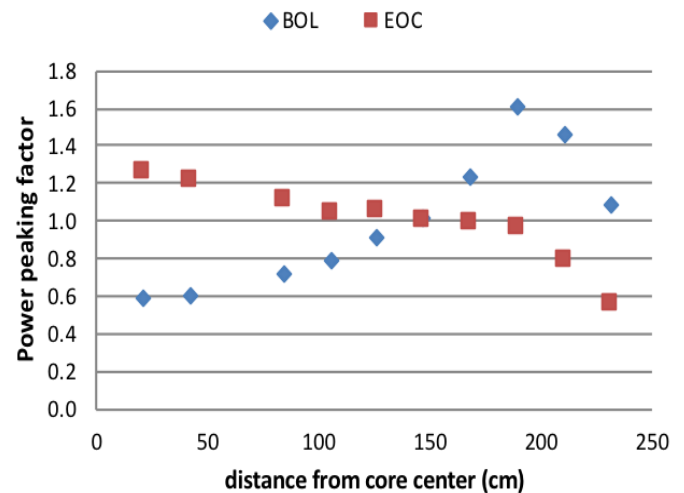

Fig. (4): Radial power peaking of ESFR core at BOL and EOC.

3.2. Reactivity of the ESFR core

Fig. 5 shows the reactivity of ESFR core as a function of burnup time in EFPD. The reactivity decreases gradually with irradiation time due to fuel depletion and fission products accumulation, however the core continue to operate with positive reactivity (k-eff higher than 1) during the entire irradiation time (2050 EFPD). Although reactivity differentiates during the burnup, the reactivity swing ($\Delta\rho$) is small between the BOL and EOC conditions. The reactivity swing from the initial condition (BOL) to the final (EOC) is only 1080 pcm. The fluctuation of core reactivity values is attributed to the fluctuation in the contribution of the IC and OC to the total generated power (see Fig. 6). Finally, the discharged fuel burnup has reached 99 GWd/tHM at the end of burnup cycle.
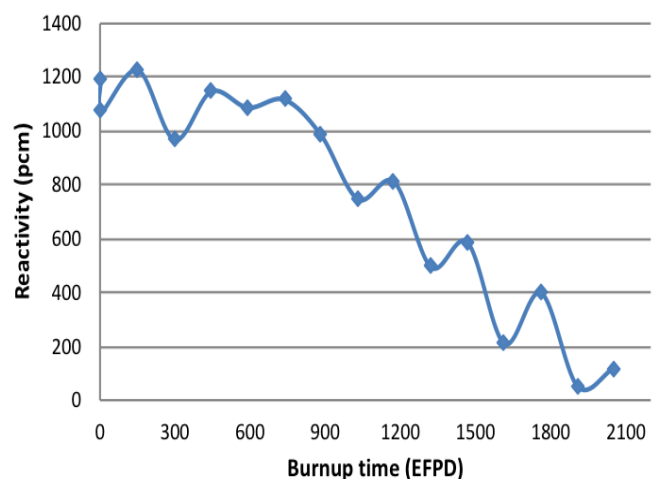

Fig. (5): The reactivity of ESFR core as a function of burnup time.

The results of MCNPX burnup calculations indicate that the contribution of IC zone to total power (averaged over fuel cycle) is higher than the OC zone. Fig. 6 shows the percentage contribution of both cores to the total core power. The fluctuation demonstrated in the contribution of both cores is attributed to the relative changes in the composition of IC and OC materials during burnup. As expected, the contribution of the OC is higher at BOL mainly due to its higher fissile content and its relatively larger number of fuel assemblies (228 FA) compared to the inner one (225 FA). However, during burnup the higher fission rat of OC combined with the higher fertile (^{238}U) content of IC result in a higher breeding rate of ^{239}Pu in IC relative to the OC and hence the IC contribution to power starts to increase due to the buildup of ^{239}Pu. The percentage contribution of the inner core (averaged over fuel cycle) to the total generated power of the core was found to be 53% versus 47% of the outer core.
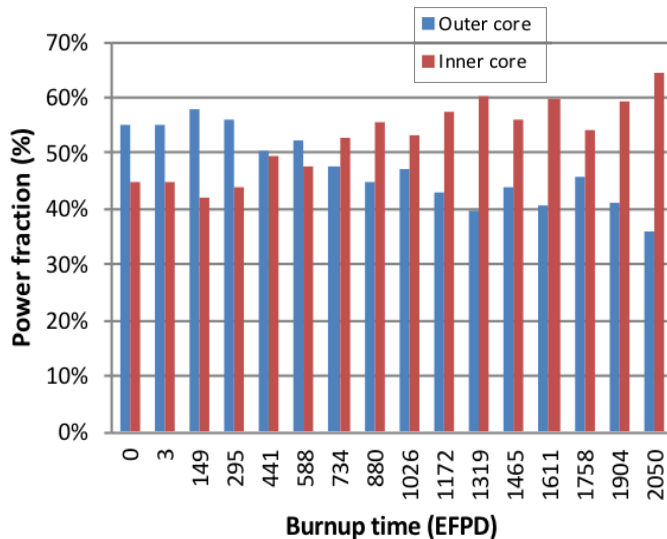

Fig. (6): Percentage contributions of OC and IC to the total generated power during fuel cycle.

3.3. Evolution of Actinides Masses

For the calculation of the nuclide inventories, the predictor/corrector method in MCNPX is followed. This method requires two criticality calculations per each burnup interval for prediction and correction steps. All the burnup calculations were performed using MCNP 2.7 with the depletion code CINDER90 which has been integrated in the MCNPX package from version 2.6.0. The integration of CINDER90 into the MCNPX Monte Carlo transport code provided a self-contained Monte Carlo-linked depletion capability **[14]**.

Fig. 7 presents the mass evolution of the main fuel components namely, ^{238}U, ^{235}U, total plutonium (Total Pu: the mass sum of ^{239}Pu, ^{241}Pu, ^{238}Pu, ^{240}Pu and ^{242}Pu

isotopes) and total minor actinides (MA: the mass sum of Np, Am, and Cm isotopes). It can be seen that the mass of ^{235}U decrease gradually during burnup mainly due to fission. On the other hand, the total plutonium mass is almost constant during irradiation time. This indicates that on average fission rates of Pu isotopes is almost equal to their breeding from present fertile isotopes (mainly ^{238}U isotope). By the end of fuel cycle (2050 EFPD), the total plutonium content in the ESFR core is increased by 277 kg. A 90% of this mass increase is ^{239}Pu and 10% is ^{240}Pu. Meanwhile, Fig. 7 shows that, the total mass of MA increase gradually during burnup. This increase is mainly due to the transmutation of ^{238}U as well as Pu isotopes through neutron capture. The MA increase from 92 kg (of ^{241}Am) at BOL to 412 kg by the end of burnup cycle which represents only about 0.61 w% of the EOC actinide inventory. This mass of MA is mainly attributed to ^{241}Am originating in fresh fuel and through transmutation (see Fig. 9), and also to the pile-up of Np, and Cm isotopes during core operation.
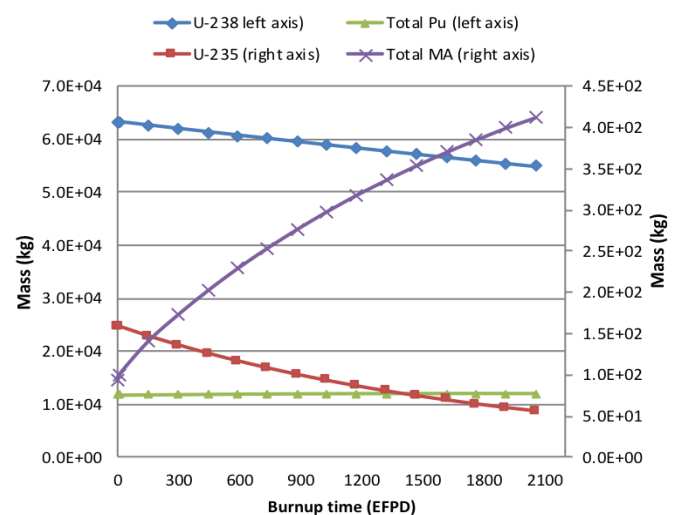

Fig. (7): Mass evolution of the main fuel components of the ESFR core.

Fig. 8 shows the mass evolution of the plutonium vector (^{239}Pu, ^{241}Pu, ^{238}Pu, ^{240}Pu, and ^{242}Pu isotopes). As ^{239}Pu, and ^{240}Pu are the main contributors to the composition of Pu vector, the change in the total plutonium mass is predominated by their fission rates and breeding from present fertile nuclides. As shown, the mass of the fissile isotope ^{239}Pu increases gradually due to its breeding from the fertile isotopes ^{238}U. On the other hand, the mass of ^{240}Pu increases due to ^{239}Pu transmutation through neutron capture. By the end of burnup time the masses of ^{239}Pu and ^{240}Pu increase by 16.5% and 1.8%, respectively. On the other hand, the masses of the other Pu isotopes (^{238}Pu, ^{241}Pu and ^{242}Pu)

decrease during burnup through fission or transmutation by neutron capture. As ^{239}Pu isotope is the major contributor to the ESFR core fissile mass (sum of ^{235}U, ^{239}Pu, and ^{241}Pu masses), the total fissile content of the core increases during burnup by 7% due to the buildup of ^{239}Pu through breeding from ^{238}U. At the EOC the mass of ^{239}Pu will represent 91% of the core fissile content.
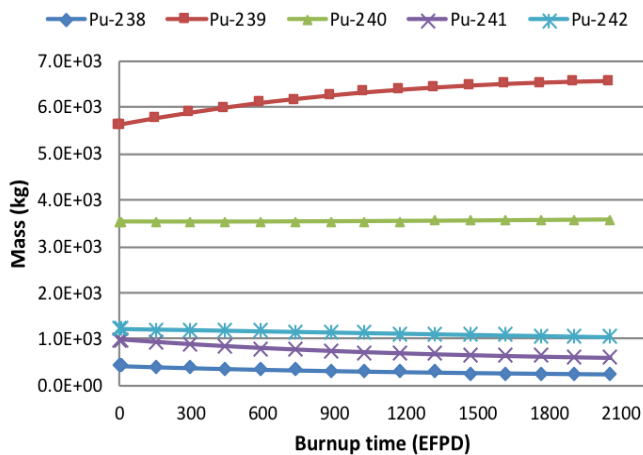

Fig. 8: Mass evolution of plutonium isotopes.

Fig. 9 shows the mass evolution of the total MA and the main MA contributors namely, Np (sum of all Np isotopes masses), Am (sum of all Am isotopes masses), and Cm (sum of all Cm isotopes masses) as a function of core operation time in EFPD. It is clear that, the evolution of the MA in the core is dominated by Am buildup mainly ^{241}Am whereas the components of ^{241}Am and ^{241}Pu play an important role in it, as these two nuclides are interconnected through the transmutation and decay. The total MA content (relative to the total fuel mass) increases from 0.12% at BOL to 0.61% at EOC and the minor actinides vector at the end of irradiation period is composed mainly from Am, Cm and Np, with weight percentages of 73%, 16% and 11%, respectively.
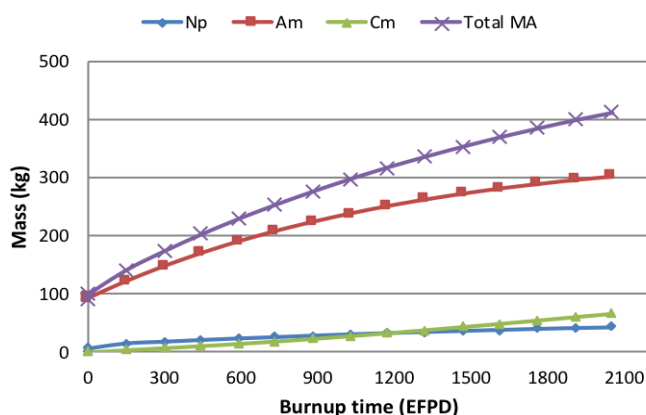

Fig. (9): The mass evolution of the main MA components.

4. CONCLUSIONS

A number of fuel burnup related parameters have been calculated for the ESFR oxide-fuelled core with the help of the Monte Carlo MCNP computational code. These included the radial flux and power distributions in the ESFR core and reactivity changes during operation as well as the evolution of fuel composition inside the ESFR core. The power peaking factor was evaluated both for the beginning of life as well as the end of cycle situations, to take into account the changes in fuel composition during burnup. The results prove that the design objective to flatten the radial power profile in the core was fulfilled in particular at EOC as the power profile is much more flattened at EOC rather than BOL (Fig. 4). Although reactivity differentiates during the burnup, the reactivity swing ($\Delta\rho$) is small between BOL and EOC conditions. The reactivity drop from the initial condition (BOL) to the final (EOC) is only 1080 pcm. This is due the efficient breeding of the fissile isotope ^{239}Pu within the ESFR core. By the end of fuel cycle, the ^{239}Pu mass is increased by 16.5 w% of its initial mass and the total fissile content of the core is increased by 7.0 w%. The obtained results indicate that ESFR operates as a breeder reactor and that this core can achieve sustainability with breeding ratio above 1.0. Moreover, by the end of burnup cycle the total MA content represents only about 0.61 w% of the fuel inventory mass at end of cycle. These results can be used as first step for future detailed assessments of fuel characterization and performance evaluation of ESFR core.

REFERENCES

[1] OECD Nuclear Energy Agency, 2008. Generation IV International Forum Annual Report

[2] A. Làzaro, L. Ammirabile, G. Bandini, G. Darmet, S. Massara, P. Dufour, A. Tosello, E. Gallego, G. Jimenez, K. Mikityuk, M. Schikorr, E. Bubelis, A. Ponomarev, R. Kruessmann and M. Stempniewicz, "Code assessment and modelling for Design Basis Accident Analysis of the European sodium fast reactor design. Part I: System description, modelling and benchmarking," Nuclear Engineering and Design, vol. 266, pp. 1-16, 2014.

[3] M. Xu, Chinese fast reactor technology development. In: The 5th Nuclear Energy Symposium on Energy Future in the Asia/Pacific Region, Beijing, 2000, pp. pp. 28-37.

[4] O. Saraev, Y. Noskov, D. Zverev, B. Vasilev, V. Sedakov, V. Poplavskii, A. Tsibulya, V. Ershov

and S. Znamenskii, "BN-800 design, validation and construction status," Atomic Energy, vol. 108, no. 4, pp. 248-253, 2012.

[5] S. Chetal, V. Balasubramanuan, P. Chellapandi, P. Mohanakrishnan, P. Puthiyavinayagam, C. Pillai, S. Raghupathy, T. Shanmugham and C. Sivathanu Pillai, "Design of prototype fast breeder reactor," Nuclear Engineering and Design, vol. 236, no. 7-8, pp. 852-860, 2006.

[6] A. Vasile, "The Collaborative Project for a European Sodium Fast Reactor CP ESFR," in In: Proceedings of the 11th International Congress on Advances in Nuclear Power Plants, Nice, France, 2011.

[7] Pelowitz, D.B., 2011. MCNPX User's Manual Version 2.7.0. Los Alamos National Laboratory, U.S., April 2011, LA-CP-11-00438.

[8] L. Ammirabile and H. Tsige-Tamirat, "Pre-conceptual thermalhydraulics and neutronic studies on sodium-cooled oxide and carbide cores," Annals of Nuclear Energy, vol. 60, pp. 127-140, 2013.

[9] D. Blanchet and L. Buiron, ESFR Working Horse description, Cadarache, 2009

[10] A. Facchini, V. Giusti, R. Ciolini , K. Tucek, D. Thomas, E. D'Agata, "Detailed neutronic study of the power evolution for the European Sodium Fast Reactor during a positive insertion of reactivity". Nuclear Engineering and Design 313 (2017) 1–9.

[11] R. MacFarlane and A. Kahler, "Methods for Processing ENDF/B-VII with NJOY," Nuclear Data Sheets, vol. 111, pp. 2739-2890, 2010.

[12] X-5 Monte Carlo Team, 2003. MCNP - A general Monte Carlo N-particle Transport code, Version 5, LA-UR-03-1987.

[13] L. Snoj and M. Ravnik, "Calculation of Power Density with MCNP in TRIGA reactor," in In proceedings of Nuclear Energy for New Europe 2006, Portoroz, Slovenia, 2006.

[14] B. Denise, D.B. Pelowitz, J.W. Durkee, J.S. Elson, M.L. Fensin, J.S. Hendricks, M.R. James, R.C. Johns, G.W. McKinney, S.G. Mashnik, J.M. Verbeke, L.S. Waters, T.A.Wilcox, . MCNPX 2.7.0 Extensions. LA-UR-11-02295 (2011).